

Evaluation of Moonpool Effects on Hydrodynamic Resistance of a Supply Vessel, Using Experimental and Numerical Methods

Mohammad Shahabadi¹, Arash shadlaghani^{2*}, Shahriar Mansoorzadeh³

¹ Department of Mechanical Eng.; Isfahan Univ. of Tech.; Shahabadi_mohammad@yahoo.com

^{2*} Department of Mechanical Eng.; Isfahan Univ. of Tech.; A.shadlaghani@me.iut.ac.ir

³ Subsea Science & Technology Institute; Isfahan Univ. of Tech.; Shahriar@cc.iut.ac.ir

ARTICLE INFO

Article History:

Received: 1 Jan. 2017

Accepted: 15 Mar. 2017

Keywords:

Ship Resistance

Moonpool

Towing Tank Tests

CFD Simulation

ABSTRACT

Moonpool is an opening in the floor or base of a hull ship which can be used to lower tools and vehicles into the sea in a protected area. In this paper, the effect of a rectangular cross section moonpool on the resistance force of a supply vessel was investigated both by experimental and numerical methods. For both methods a 1:37.2 scale of Caspian3 surface vessel was used. Experiments were carried out at various Froude numbers in the range of 0.185-0.370 in the towing tank for cases with moonpool, i.e, when the entrance at the bottom of the ship was open and without moonpool, i.e, when the entrance was closed. A two phase flow CFD simulation based on volume of fluid (VOF) method was used to calculate the resistance coefficients of the vessel and to investigate fluid flow around the ship and inside the moonpool. The acquired numerical results showed fair agreement with the experimental results. The results showed that the resistance coefficient of the ship with moonpool was about 21 percent larger than that of the ship without moonpool.

1. Introduction

Moonpool is a wetted opening, located near the mid-ship, which allows researchers take their tools and instruments into the water in a safer and more protected environment. Surface vessels are sometimes equipped with moonpool. It affects the motion resistance by changing the patterns of fluid flow around the vessel. There are two reasons for water motion inside the moonpool: the first is the forward speed of the vessel in transit mode and the second is when waves are approaching the vessel in operating mode, at zero speed. The motion appears as two modes of oscillations including vertical motion of the water column (heave) and water movement between the vertical walls in longitudinal direction (surge) as shown in Figure 1. These oscillations are called piston and sloshing modes, respectively. More details were clarified by Hammargren and Törnblom [1].

Various methods have been used to predict the hydrodynamic behavior of surface vessels and moonpools' effects. For example, Veer and Tholen [2] experimentally found that the moonpool increased the total resistance of a vessel about 10%-60% at various velocities. They also investigated the various length/width ratios of the moonpool for decreasing oscillations in the moonpool. Albers [3] developed a

mathematical model describing the relative motions of water inside a moonpool. He also carried out experiments for a test model to obtain empirical results and compared them together. Fredriksen-Kristiansen and Faltinsen [4] experimentally studied the behavior of piston-mode resonance in a moonpool at low current speed and compared their results with a nonlinear hybrid method coupled potential and viscous flow. They concluded that the moonpool behavior significantly depends on the heave forcing amplitude. Liu-Zhou and Tang [5] investigated the heave responses of a truss Spar platform with semi-closed moonpool in random waves. The results showed that water motions inside the moonpool significantly affected the platform heave when the characteristic wave period is far away from the natural period of the platform heave motion. Matusiak [6] theoretically evaluated the motion of a water column in the moonpool of a ship and compared his results by experimental method. He obtained his results for both closed and open moonpool conditions. Nevertheless, a few numerical works have been published to investigate the effects of moonpool in comparison to experimental works. For instance, Sadigh and Xiang-Liang [7] performed a numerical research to obtain the pressure coefficient in circular and square

moonpools. Alsgaard [8] investigated four different configurations of the moonpool using OpenFOAM tool. Numerical verification was firstly accomplished on an experiment of a 2D section of a moonpool in shallow water. Wang–Liqin and Tang [9] numerically investigated square-ring and crisscross shapes of a moonpool entrance on the motion form of fluid and mass flow rate in the moonpool for hard tank of a truss spar.

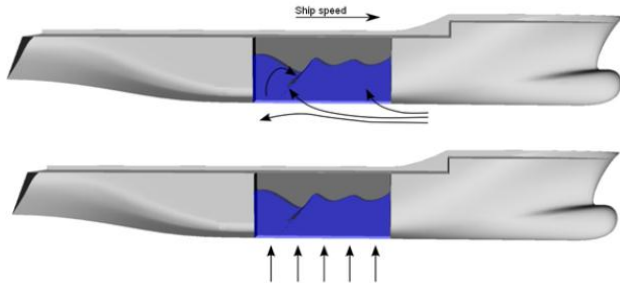


Figure 1. Water motion in the moonpool for sloshing mode (top) and piston mode (bottom)

One of the main effects of a moonpool is the increase of ship resistance. As mentioned above, this effect was studied either by numerical methods or by experimental techniques. The aim of this paper was to use both experimental and numerical methods to investigate the amount and reasons of increasing the total resistance of a supply vessel called Caspian3. The commercial computational fluid dynamics code, CFX, was used to model the motion of the ship in a two phase flow domain. In order to study this problem experimentally, a model with a scale of 1:37.2 was built and various tests conducted in IUT towing tank. Figure 2 shows the sketch of this vessel indicating its moonpool location.

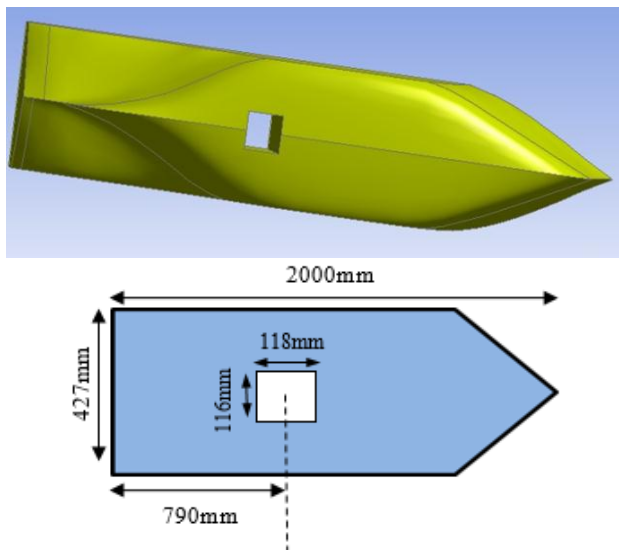


Figure 2. Sketch of vessel and its moonpool location

2. Dimensional Analysis

By the use of dimensional analysis, the forces and moments measured in a towing tank tests on a scaled model of a ship can be used to predict the corresponding forces and moments related to the full

scale ship. Dynamic similarity between the model and real ship can be achieved if Froude (Fr) and Reynolds (Re) numbers of the full scale and model ship are equivalent. If the towing tests are performed in a water with the same properties as the sea water, then:

$$Re_s = Re_m \rightarrow \left(\frac{VL}{\nu}\right)_s = \left(\frac{VL}{\nu}\right)_m \rightarrow (VL)_s = (VL)_m \quad (1)$$

$$Fr_s = Fr_m \rightarrow \left(\frac{V}{\sqrt{gL}}\right)_s = \left(\frac{V}{\sqrt{gL}}\right)_m \rightarrow \left(\frac{V}{\sqrt{L}}\right)_s = \left(\frac{V}{\sqrt{L}}\right)_m \quad (2)$$

where, V and L are the speed and length of the ship, respectively. Subscripts s and m refer to the full scale ship and model, respectively. The same Froude number in model and full scale (Froude's law) requires that:

$$V_m = \frac{V_s}{\sqrt{\lambda}} \quad (3)$$

Where, λ is the scale factor. While, the same Reynolds number in model and full scale would result in:

$$V_m = \lambda V_s \quad (4)$$

These two equations can be satisfied simultaneously only if $\lambda=1$, which means that, it is not possible to scale down the ship dimensions and to perform the tests in a towing tank. To overcome this problem, Froude theorem was used, in which, it is assumed that the total resistance coefficient defined as:

$$C_T = \frac{R_T}{0.5\rho V^2 A_w} \quad (5)$$

Eq. (5) can be divided into two parts: friction coefficient, C_F , which is a function of Reynolds number and residuary coefficient, C_R , which is a function of Froude number, that is

$$C_T(Re, Fr) = C_F(Re) + C_R(Fr) \quad (6)$$

where, R_T is the total resistance force, A_w is the wetted area of the ship, ρ is the density, and V is the ship velocity. Friction resistance coefficient of the ship can be calculated from the following empirical (1975):

$$C_F = \frac{0.075}{(\log_{10} Re - 2)^2} \quad (7)$$

C_R can be obtained from Eq. (6), in which C_T is calculated by measuring the resistance force of the model, R_T , towed at velocity V in a towing tank test using Eq. 5, and C_F can be calculated from Eq. 7. The key point in this method is that C_R of the model and full scale ship are equal, because $Fr_s = Fr_m$.

3. Resistance of real ship

ITTC78 method is the prevalent empirical procedure for calculating the resistance of ships. According to the ITTC78 method [10], the follow equation is used to calculate the total resistance coefficient of the real ship:

$$C_T = (1+k)C_F + C_R + C_{AA} + \Delta C_F + C_A \quad (8)$$

where, K is the form factor of the ship. C_F , in this equation, should be calculated at full scale ship Reynolds number. C_R is obtained from the model towing tank test. C_{AA} and ΔC_F are the air resistance and roughness coefficients of the real ship defined as:

$$C_{AA} = 0.001A_T / S \quad (9)$$

$$\Delta C_F = [105(\frac{k_s}{L_{wl}})^{1/3} - 0.64] \times 10^{-3} \quad (10)$$

where, A_T and S are the projected area of the ship exposed to the air flow and wetted area of the hull, respectively. k_s is the roughness of the hull, which is almost equal to $150\mu m$, and L_{wl} is the wetted length of the ship. C_A is the correlation factor in which the effect of non-equivalent Reynolds number and uncertainly analysis are imposed.

4. Experimental Test

The towing tank tests were carried out for the model in the Subsea R&D Center of the IUT. The length, width, and depth of the towing tank were $108m$, $3m$, and $2.2m$, respectively. The Froude number ranged from 0.18 to 0.37 .



Figure 3. Ship model attached to dynamometer

A three component load cell was used to measure the resistance forces and moments of the model. The load cell was located at the longitudinal center of gravity (LCG) and in the line of the expected thrust line. The model is fixed in heave, trim and yaw. This allows the load cell to measure the axial and lateral forces, as well as yaw moment, however, only the axial measured forces are used in the present work. In order to monitor the wave profile and wetted surface around the model hull, horizontal and vertical lines were drawn on a water proof paper and attached on the hull model surface. Two digital cameras, then, were used to film and capture the wave profile.

Required time between successive runs was at least 20 minutes. Experiments were performed for bare hull without considering the propeller and other appendages.

5. Numerical simulation

The volume of fluid (VOF) technique was used to approximate the free surface flow because both fluids (air and water) were considered as continuous fluids. Two-phase Reynolds averaged Navier-Stokes (RANS) equations were employed to obtain the flow variables as follow:

$$\alpha_i = \frac{V_i}{V} \quad i = 1, 2 \quad (11)$$

$$\mathbf{V}_i = \mathbf{V} \quad (12)$$

$$\sum_i \nabla \cdot (\alpha_i \mathbf{V}) = 0 \quad (13)$$

$$\frac{\partial}{\partial t} (\alpha_i \rho_i) + \nabla \cdot (\alpha_i \rho_i \mathbf{V}) = 0 \quad (14)$$

$$\frac{\partial}{\partial t} (\rho_m \mathbf{V}) + \nabla \cdot (\rho_m \mathbf{V} \times \mathbf{V}) = \nabla \cdot (-P + \mu_m ((\nabla \mathbf{V}) + (\nabla \mathbf{V})^T)) \quad (15)$$

Eqs. (11-13) demonstrate volume conservations in each element. In the above equations, V is the velocity vector, α_i is the volume fraction of phase i , V_i is the volume of phase i , V is the total volume, ρ_m and μ_m are the bulk density and viscosity, respectively, and finally P is the pressure acting on the flow.

The effect of surface tension was overlooked and two phases didn't mix together at interface. The volume fraction of phases was zero or one in the entire domain except at the interface of water-air. Because of turbulence nature of fluid flow, it's essential to model the created Reynolds stresses in the RANS equations to close the governing equations. Turbulence models related the apparent unknown terms ($\rho u'_i u'_j$) and known flow variables together.

Hereby, $K-\epsilon$ model was used for simulations because this model is robust in modeling the Reynolds stresses in the wide range of engineering applications.

The finite volume method was used to solve the NS equations and volume fraction equations numerically, and high resolution scheme was also used to discretize the advection and turbulence terms. Residual target was set at 10^{-5} for all governing equations in order to achieve convergence.

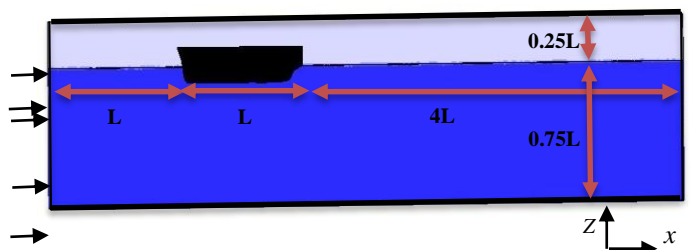


Figure 4. Domain and used boundary conditions of fluid domain

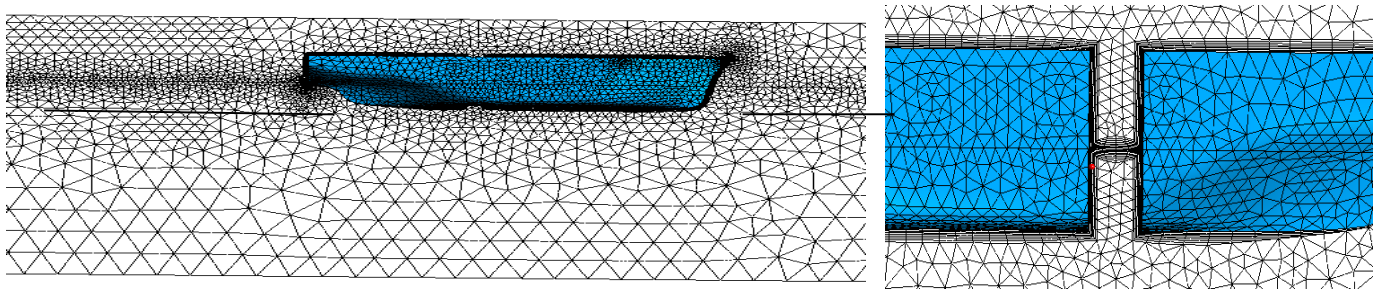


Figure 5. Unstructured grids on the ship hull and inside the rectangular-shaped moonpool

Table 1. Typical grid study for the ship model based on the skin drag coefficient

| Element No | 635416 | 858638 | 1300050 | 1464538 | 2038408 | 2543545 |
|------------|--------|--------|---------|---------|---------|---------|
| C_f | 0.0045 | 0.0043 | 0.0041 | 0.00405 | 0.00403 | 0.00403 |

5.1. Computational domain & boundary condition

After investigating various dimensions for computational domain, a cubic domain was established as Figure 4. The boundary condition set as constant velocity for the inlet. The free slip wall condition was used for lateral walls, and non-slip wall condition was used for the ship surface. The static pressure condition was used for outlet. Because of the sheer symmetry of the ship, only half of the fluid domain was used for simulations.

5.2. Mesh definition

Unstructured grids were generated in the fluid domain for all simulation. In addition, the density of grids should be more increased near the free surface and ship surface in order to capture the free surface waves and large gradients flows. Prism elements were used to increase the number of elements and consequently accuracy of the solution in these regions.

As a result, it's required to estimate the total boundary layer thickness and the first layer thickness created around the model as [11]

$$\delta = 0.035LRe^{-1/7} \tag{16}$$

$$\Delta y = Ly^+ \sqrt{80} Re^{-13/4} \tag{17}$$

For example, when the ship model moves with a constant velocity of 1.6m/s, the total thickness is about to 27mm. On the other hand, the first layer thickness for a desired y^+ of 30 is equivalent to 2.5mm. So that, 8 prism layers with expansion factor of 1.1 cover the boundary layer, totally.

The feature of boundary layer meshing was similar around the ship model in the water and air domains for discarding the effect of mesh difference on the output results.

In order to ensure that the quality of generated elements was acceptable, a grid study was performed. The grid study was accomplished in a way that the variation of friction coefficient should be negligible with increasing the number of elements. Table 1 shows these variations versus number of elements.

According to table 1, variations of friction coefficient approximately remain at a constant value of ≈ 0.004

with more increment of elements number; therefore, the computational time can be decreased by choosing the optimum meshing (Fine2) with lower elements.

6. Estimation of hydrodynamic resistance

The steady towing tests were conducted for accessing the resistance coefficients, pressure distribution, and wave profile at various velocities.

By measuring the forces acted on the model ship in the experiments and simulations, the total resistance coefficient (C_T) can be calculated according to the Eq. 5. Note that, it's also possible to calculate the friction force in CFD analysis, which would be compared to the empirical formula provided in Eq. 7. The resistance coefficients are shown in table 2 and 3 in the mentioned range of Froude numbers for closed and open moonpool conditions.

According to the obtained experimental and numerical results presented in these tables, the total resistance coefficient of the ship, with closed and open moonpool, increases with Froude number. The resistance coefficients of the ship model with open moonpool are larger than those with closed moonpool, at the same Froude numbers. As shown in these tables, the results obtained for the total resistance coefficients with experimental facility are always larger than the corresponding values obtained by the numerical study. One of the main reasons for this difference is the use of turbulence stimulator in the ship model experiments, which is used to make the flow field turbulent. The turbulence stimulator was attached to the model ship in order to create more similarity conditions between the model and ship flow field.

It is important to realize that how the moonpool increase the total resistance of the ship model by investigating the behavior of friction and residuary coefficients for various Froude numbers.

It should be noted that comparing the values of C_F with and without moonpool in these tables could be misleading since the wetted area, appeared in Eq. 7, for the open moon pool slightly differs from that for the closed moonpool. This area for the open moonpool, comparing to the area for the closed

moonpool, includes two extra lateral walls (left and right walls of the moonpool) and lacks the bottom moonpool wall. The wetted area of the model ship was about $1.204m^2$ and $1.19 m^2$ for closed and open moonpool, respectively. Frictional force in x direction, R_{fx} , can be calculated numerically as:

$$R_{fx} = \int \tau_w dA_x \quad (18)$$

Table 2 and 3 also show that the difference between the friction coefficients obtained by Eq. 7 with those obtained by numerical values is larger for the ship model with moonpool than for the ship model without moonpool. This can be related to the fact that the presence of moonpool is not predicted in empirical Eq. 7 and it yields the same friction factor for the ships with and without moonpool, which is physically not acceptable. However, we will show that using Eq. 7 will not introduce a large error in evaluating the total resistance of the real ship. Table 3 shows that while the results obtained for the

friction resistance coefficient of the ship model using Eq. 7, is up to 20 percent larger than the corresponding values obtained by the numerical study, this difference for the residuary resistance coefficient, which will be used to estimate the total resistance coefficient of the real ship, is less than 9.5 percent. This is due to the lower contribution of friction coefficient into the total resistance coefficient. Since the Reynolds number for the real ship is much larger than that of the model, the friction coefficient of the real ship will be even smaller, while the total resistance coefficient of the ship is larger. The contribution of friction coefficient into the total resistance coefficient for both model and ship, with/without moonpool, is shown in table 4. In order to calculate the friction coefficient of the ship, the following equation is used:

$$\frac{(C_F)_s}{(C_F)_m} = \frac{(\log_{10}^{(Re)_m} - 2)}{(\log_{10}^{(Re)_s} - 2)} = \frac{(\log_{10}^{(Re)_m} - 2)}{(\log_{10}^{2^{1.5}(Re)_m} - 2)} \quad (19)$$

Table 2. Resistance coefficients computed by experimental and numerical methods without moonpool

| Fr. No | $C_T _{Closed} \times 10^2$ | | Difference (percent) | $C_F _{Closed} \times 10^2$ | | Difference (percent) | $C_R _{Closed} \times 10^2$ | | Difference (percent) |
|--------|------------------------------|-------|----------------------|------------------------------|-------|----------------------|------------------------------|-------|----------------------|
| | Exp. | CFD | | Eq. (5) | CFD | | Exp. | CFD | |
| 0.185 | 0.712 | 0.683 | 4.073 | 0.432 | 0.362 | 16.203 | 0.280 | 0.321 | 12.772 |
| 0.232 | 0.731 | 0.692 | 5.335 | 0.423 | 0.353 | 16.548 | 0.308 | 0.339 | 9.144 |
| 0.255 | 0.768 | 0.701 | 8.724 | 0.411 | 0.348 | 15.328 | 0.358 | 0.353 | -1.133 |
| 0.278 | 0.873 | 0.741 | 15.12 | 0.402 | 0.342 | 14.925 | 0.471 | 0.399 | -18.045 |
| 0.324 | 1.072 | 0.952 | 11.194 | 0.388 | 0.331 | 14.690 | 0.684 | 0.621 | -10.145 |
| 0.37 | 1.254 | 1.101 | 12.201 | 0.369 | 0.321 | 13.008 | 0.885 | 0.780 | -13.462 |

Table 3. Resistance coefficients computed by experimental and numerical methods with moonpool

| Fr. No | $C_T _{Open} \times 10^2$ | | Difference (percent) | $C_F _{Open} \times 10^2$ | | Difference (percent) | $C_R _{Open} \times 10^2$ | | Difference (percent) |
|--------|----------------------------|-------|----------------------|----------------------------|-------|----------------------|----------------------------|-------|----------------------|
| | Exp. | CFD | | Eq. (5) | CFD | | Exp. | CFD | |
| 0.185 | 0.810 | 0.771 | 4.814 | 0.432 | 0.352 | 18.518 | 0.378 | 0.419 | 9.785 |
| 0.232 | 0.835 | 0.784 | 6.107 | 0.423 | 0.342 | 19.148 | 0.412 | 0.442 | 6.787 |
| 0.255 | 0.891 | 0.825 | 7.407 | 0.411 | 0.329 | 19.951 | 0.480 | 0.496 | 3.225 |
| 0.278 | 0.987 | 0.876 | 11.246 | 0.402 | 0.323 | 19.651 | 0.585 | 0.553 | -5.787 |
| 0.324 | 1.322 | 1.160 | 12.254 | 0.388 | 0.312 | 19.587 | 0.934 | 0.848 | -10.142 |
| 0.37 | 1.477 | 1.339 | 9.343 | 0.369 | 0.301 | 18.428 | 1.108 | 1.038 | -6.744 |

Table 4. Contribution of friction coefficient into the total resistance coefficient for both model and ship, with/without moonpool

| Fr. No | $\left(\frac{C_F}{C_T}\right)_m$ | | $\left(\frac{C_F}{C_T}\right)_m$ | | $\left(\frac{C_F}{C_T}\right)_s$ | | $\left(\frac{C_F}{C_T}\right)_s$ | |
|--------|----------------------------------|------|----------------------------------|------|----------------------------------|-------------|----------------------------------|-------------|
| | without moonpool | | with moonpool | | without moonpool | | with moonpool | |
| | Eq. (5)+Exp | CFD | Eq. (5) | CFD | Eq. (5)+Exp | Eq. (5)+Exp | Eq. (5)+Exp | Eq. (5)+Exp |
| 0.185 | 0.61 | 0.53 | 0.53 | 0.46 | 0.24 | 0.24 | 0.31 | 0.31 |
| 0.232 | 0.58 | 0.51 | 0.51 | 0.44 | 0.23 | 0.23 | 0.29 | 0.29 |
| 0.255 | 0.53 | 0.50 | 0.46 | 0.40 | 0.22 | 0.22 | 0.26 | 0.26 |
| 0.278 | 0.46 | 0.46 | 0.40 | 0.37 | 0.19 | 0.19 | 0.22 | 0.22 |
| 0.324 | 0.36 | 0.34 | 0.29 | 0.27 | 0.15 | 0.15 | 0.15 | 0.15 |
| 0.37 | 0.3 | 0.29 | 0.25 | 0.23 | 0.13 | 0.13 | 0.13 | 0.13 |

The total resistance coefficient of the ship was obtained by ignoring $K, C_{AA}, \Delta C_F,$ and C_A in Eq. 8, because these parameters had the same values for the ships with and without moonpool and the main aim of the present study is to investigate the difference between the total resistance of the ships with and without moonpool. Therefore, we consider:

$$C_T|_s = C_R + C_F|_s \quad (20)$$

The magnitudes of $(C_F)_k$ in the above equation are obtained by Eq. 7. The magnitudes of C_R for the model and the real ship are equal, at same Froude numbers, and can be obtained from table 2 and 3 for both open and closed moonpool. As shown in table 4, since the contribution of friction coefficient into the total resistance coefficient for the real ship is much lower than that for the model ship, using Eq. 7 will not introduce significant difference between the experimental and numerical results for the total resistance coefficient.

The results for the total resistance coefficients obtained both by experimental and numerical methods showed that presence of moonpool increases the residuary coefficients of the ship model.

This is due to the flow pattern introduced inside the moonpool. Comparing the results obtained for the residuary coefficients shown in Tables 2 and 3 indicates that, as the Froude number increases, the difference between the residuary coefficient of the

model ship with and without moonpool also increases.

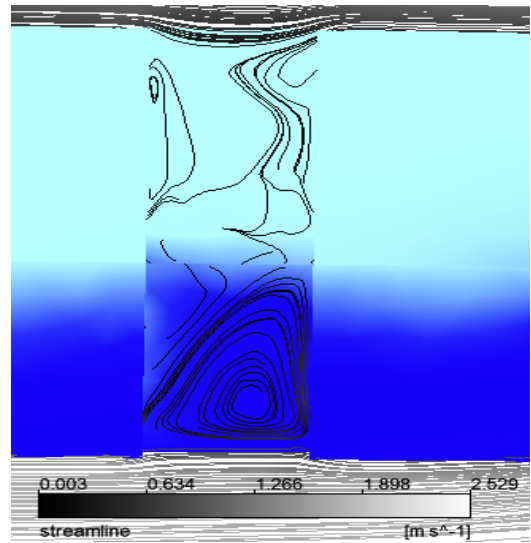


Figure 6. The water velocity streamline inside the moonpool

This is due to the increase of water circulation inside the moonpool, as the Froude number (ship speed) increases. The generated circulation in the liquid phase inside the moonpool is indicated in Figure 6. Water circulation inside the moonpool and interaction of water with its vertical walls produces a high pressure zone inside the moonpool. Pressure contours of the ship surface and the moonpool walls are shown in Figure 7.

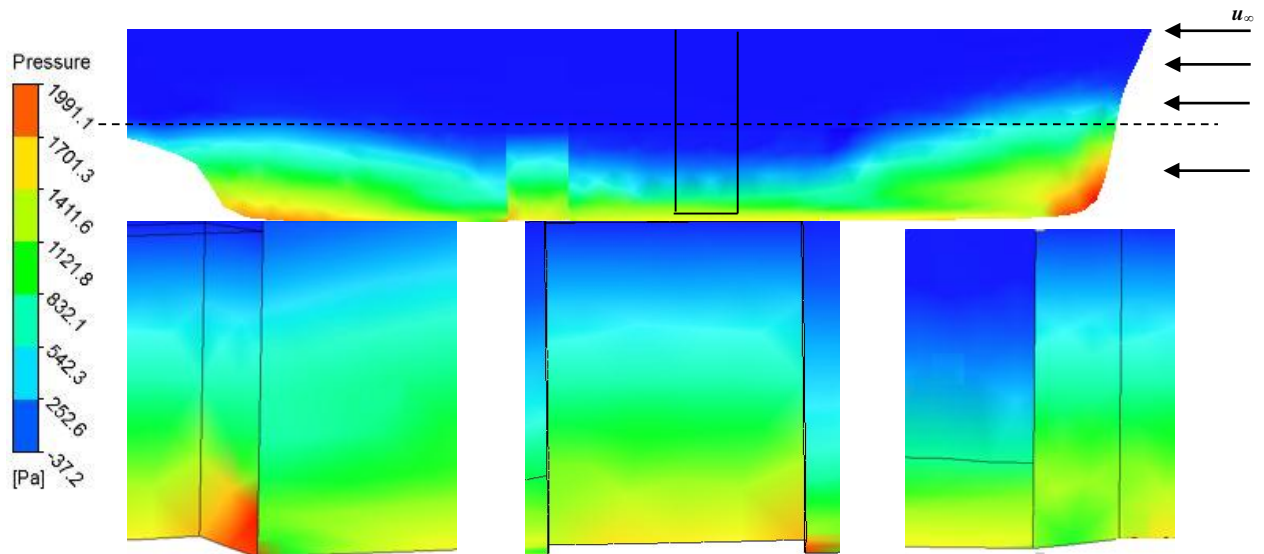


Figure 7. Pressure distribution on the moonpool internal walls
Left: Backward surface, Center: Middle surface, Right: Forward surface

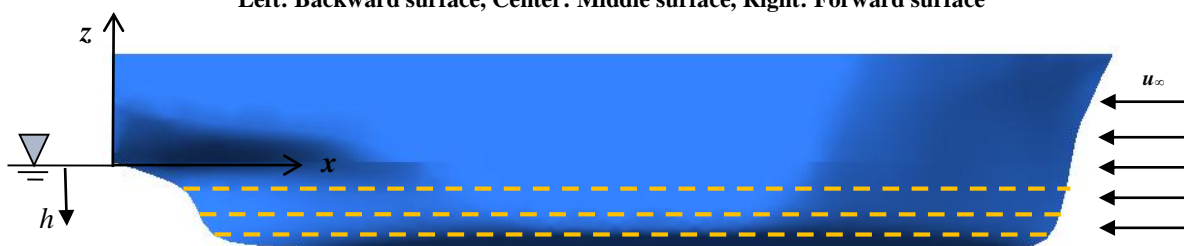


Figure 8. position of chosen lines for drawing of C_p

The high pressure area appeared on the right wall of the moonpool increases the total resistance of the ship. In order to compare the pressure distributions on the ship surface with and without moonpool, the pressure coefficient defined as, $C_p = \frac{P - P_\infty}{0.5\rho V^2}$, were calculated for both cases, at three paths shown in Figure 8, at various depths along the ship length. The results are shown in Figure 9.

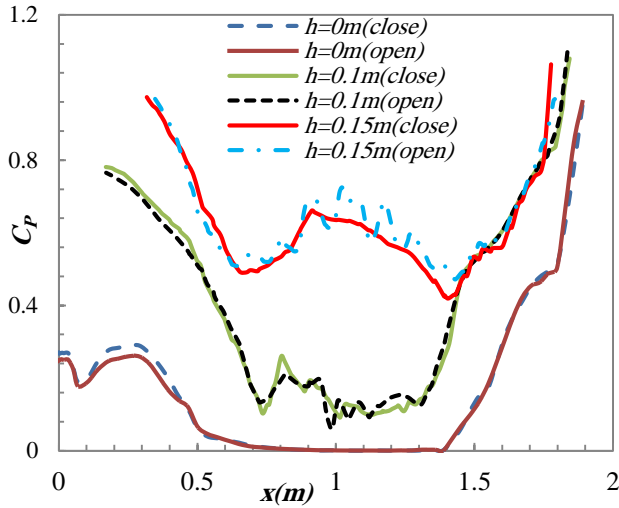


Figure 9. distribution of C_p at various depth over the ship hull at $Fr=0.37$

This figure shows that the differences between pressure coefficient distributions, with and without moonpool, along various paths on the ship hull are not significant. Therefore, the moonpool is the main location in the ship where the pressure distribution is different from that of the ship without moonpool. The total resistance force of the ship can be calculated from Eq. 5.

Table 5. Added resistance due the moonpool presence in experimental calculations

| Fr No. | $R_t _{close}$ (KN) | $R_t _{open}$ (KN) | Difference% |
|--------|---------------------|--------------------|-------------|
| 0.208 | 133 | 163 | 23.7 |
| 0.232 | 171 | 208 | 21.8 |
| 0.255 | 231 | 279 | 21.5 |
| 0.278 | 325 | 393 | 20.7 |
| 0.324 | 609 | 736 | 20.9 |

Table 5. Added resistance due the moonpool presence in experimental calculations

| Fr No. | $R_t _{close}$ (KN) | $R_t _{open}$ (KN) | Difference% |
|--------|---------------------|--------------------|-------------|
| 0.208 | 142 | 172 | 20.8 |
| 0.232 | 175 | 211 | 20.4 |
| 0.255 | 227 | 272 | 19.5 |
| 0.278 | 292 | 372 | 27.4 |
| 0.324 | 567 | 687 | 21.1 |

Table 5 and 6 compare the total resistance force obtained for the ships with and without moonpool using numerical and experimental methods. As shown in these tables, introducing the moonpool in a ship increases the total resistance force of the ship up to 23.7 percent. Unlike the friction coefficients, moonpool increases the contribution of C_R in total resistance coefficient at equivalent Froude number. Moonpool approximately increases the C_R contribution from 47 to 55 percent in the lowest Froude number, and 71 to 78 percent in highest Froude number. In brief, moonpool has a considerable effect on the residuary coefficients relative to friction coefficients, especially in higher Froude numbers. Note that, Eq. 6 has been used to calculate the residuary coefficients of the scaled model. Since the residuary coefficients of the model and the real ship are equal, at the same Froude numbers, the total resistance coefficients of the real ship can be calculated using Eq. 8. The total resistance force of the ship can, then, be calculated from equation.

7. Uncertainty Analyses

A thorough uncertainty analysis for obtaining the drag coefficient uncertainty U_{C_D} has been performed taking into account both biases errors in drag coefficient B_{C_D} (including biases in reference area B_S , velocity B_V , drag force measurement B_{F_D} and density) and precision error P_{F_D} which is obtained by repeating the experiments for $N=5$ times using the standard deviation of the results σ_{C_D} . The following equations were used to calculate the uncertainty of the drag coefficient.

$$\begin{aligned}
 (U_{C_D})^2 &= (B_{C_D})^2 + (P_{C_D})^2 \\
 (B_{C_D}^{tw})^2 &= (\theta_S B_S)^2 + (\theta_V B_V)^2 + (\theta_{F_D} B_{F_D})^2 + \\
 &+ (\theta_\rho (B_\rho + \theta_{\rho tw} B_{tw}))^2 \quad (21) \\
 P_{F_D} &= \frac{2\sigma_{C_D}}{\sqrt{N}}
 \end{aligned}$$

Where, the θ values are defined as Eq. 22. B_{F_D} , for example, includes biases in calibration of the load cell, biases of misalignment, biases of curve fitting and biases of towing tank inclination, etc. Note that t_w represents the water temperature in Eq. 22. Including all details of the above equations in the paper distract the reader from the main goal of the paper which is related to the moonpool effect on resistance coefficient of a ship. The uncertainty analysis of the current problem showed that that the maximum uncertainty value of the drag coefficient was about 0.61% of the drag coefficient value.

$$\begin{aligned} \theta_\rho &= \frac{\partial C_D}{\partial \rho} = \frac{F_D}{0.5V^2S} \left(-\frac{1}{\rho^2}\right) \\ \theta_U &= \frac{\partial C_D}{\partial V} = \frac{F_D}{0.5\rho S} \left(-\frac{2}{V^3}\right) \\ \theta_{F_D} &= \frac{\partial C_D}{\partial F_D} = \frac{1}{0.5\rho V^2S} \\ \theta_{\rho tw} &= \frac{\partial \rho}{\partial t_w} (t_w = 15^\circ c) = \\ &|0.0638 - 0.0173t_w + 0.0001897t_w^2| \end{aligned} \quad (22)$$

8. Wave profile

As shown in the previous section, pressure distributions around the ship hull with and without moonpool were almost similar. That is, the presence of moonpool did not affect the pressure distribution around the ship hull. Therefore, the wave profile around the ship hull for both cases was observed to be similar. In order to show the wave profile around the ship hull, the water volume fraction was calculated numerically. The graphical presentation of water volume fraction, which indicates the wave profile around the ship hull for various Froude number, are shown in Figure 10. As shown in this Figure, the amplitude of waves along the ship length is increased by increment of Froude numbers. The wave profiles around the ship hull was also measured experimentally and compared with the results obtained by the numerical simulations at

various Froude numbers. The wave profiles obtained, for example at Fr=0.37, are shown in Figure 11. The numerical results agreed almost well with the experimental results.

9. CONCLUSION

In this paper, the effects of introducing a rectangular cross section moonpool on the hydrodynamics resistance of a supply vessel were investigated both by experimental towing tank tests and by numerical simulations using computational fluid dynamics. It was shown that introducing the moonpool increases the resistance coefficient of the ship by more than 20 percent. This increment was mostly due to the increase of residuary coefficient, which arise from the interaction of the fluid flow with vertical walls of the moonpool and circulation of water inside moonpool. It was also demonstrated that the presence of moonpool did not affect the wave profile around the ship hull. The results obtained by the numerical simulations for the residuary coefficients of the ship with moonpool at various Froude numbers differed less than 10 percent from those obtained experimentally in the towing tank tests. One can conclude that the computational fluid dynamics can be used to investigate the effect of moonpool with various shapes, dimensions and locations on resistance of the ship with reasonable accuracy.

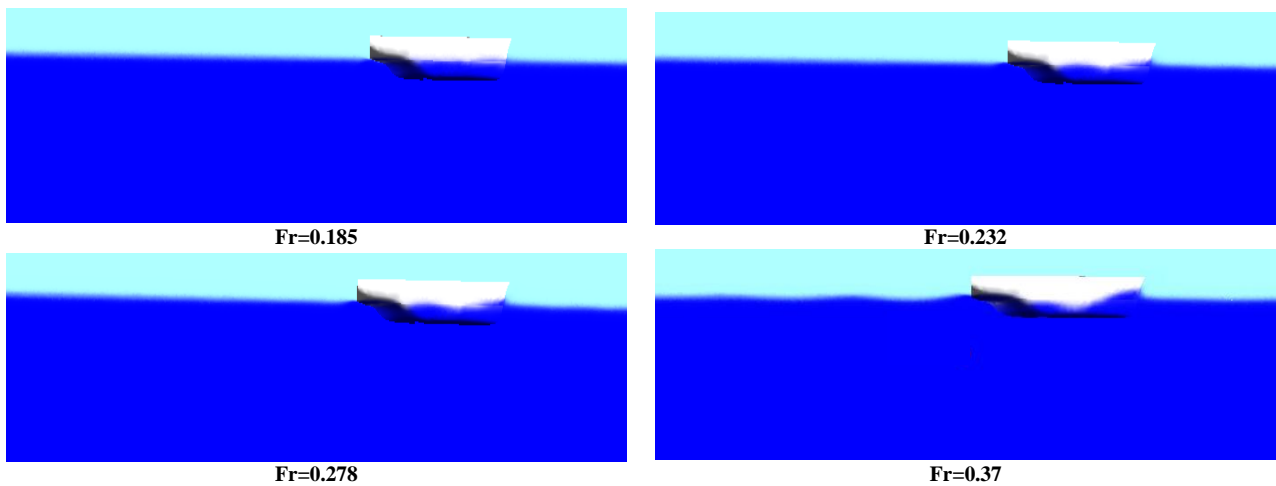


Figure 10. Water volume fraction indicating waves profile for various Froude numbers

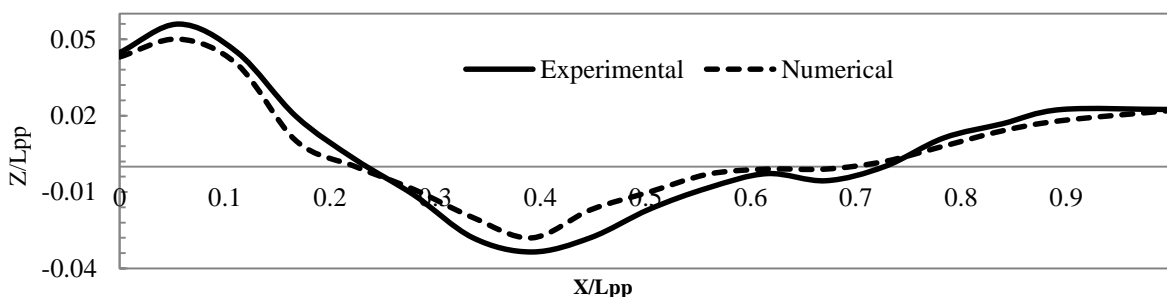


Figure 11. Comparison of waves profile over the hull at Fr=0.37

10. References

- 1- Hammargren, E., Törnblom, J., (2012), *Effect of the Moonpool on the Total Resistance of a Drillship*, Msc Thesis, Department of Shipping and Marine Technology, Chalmers University of Technology, Sweden.
- 2- Van't Veer, R., Tholen. H. (2008) *Added resistance of moonpools in calm water*, OMAE 57246, Estroil, Portugal.
- 3- Aalber, A.B., (1984), *The water motions in a moonpool*, Ocean Engineering, Vol. 11, No. 6, p. 557-579.
- 4- Fredriksen, A.G., Kristiansen, T., and and, Faltinsen, O.M., (2014), *Experimental and numerical investigation of wave resonance in moonpools at low forward speed*, Applied Ocean Research, Vol. 47, p.28–46.
- 5- Wang, B., Liu, Liqin., and Tang, Y., (2014), *CFD Simulation of the Vertical Motion Characteristics of the Moonpool Fluid for the Truss Spar*, Journal of Marine Science Application, Vol.13, p.92-98.
- 6- Matusiak, J., (1996) *Water Column Motion in a Moonpool of a Ship*, Rakenteiden Mekaniikka, Vol. 30, No. 2, p. 75-87.
- 7- Sadiq, S., Xiong-liang.Y., (2008), *Multi-Dimensional Numerical Free Surface VOF Modeling with Moonpool Experiments*, in Proceedings of the ASME 27th International Conference on Offshore Mechanics and Arctic Engineering, Estoril.
- 8- Alsgaard, J. A., (2010), *Numerical investigations of Piston mode resonance in a moonpool using Open FOAM*, M.Sc. Thesis, Department of Marine Technology, Norwegian University of Science and Technology.
- 9- Li-qin Liu., Han, Zhou., and You-gang, Tang., (2015), *Coupling response of heave and moonpool water motion of a truss Spar platform in random waves*, China Ocean Engineering, 29:2: p.169-182.
- 10- 15th ITTC, Recommended procedure performance, revision and propulsion, final release, 1978.
- 11- Shadlaghani, A., Mansoorzadeh, Sh., (2016) *Calculation of Linear Damping Coefficients by Numerical Simulation of Steady State Experiments*, journal of Applied Fluid Mechanics, Vol. 9, No. 2, p.653-660.